Journal of
Applied Crystallography
ISSN 0021-8898

Received 16 August 2006
Accepted 22 December 2006

Quantitative analysis of molecularly stacked layer structures in supported organic thin films by synchrotron grazing-incidence X-ray scattering

Jinhwan Yoon, Seungchel Choi, Sangwoo Jin, Kyeong Sik Jin, Kyuyoung Heo and Moonhor Ree*

Department of Chemistry, Pohang Accelerator Laboratory, National Research Laboratory for Polymer Synthesis and Physics, Center for Integrated Molecular Systems, and BK School of Molecular Science, Pohang University of Science and Technology, Pohang 790-784, Republic of Korea. Correspondence e-mail: ree@postech.ac.kr

In this study, we derive a grazing-incidence X-ray scattering (GIXS) formula to analyze quantitatively GIXS patterns for molecularly stacked layer structures in substrate-supported nanoscale thin films. We apply this formula in the quantitative analysis of GIXS patterns obtained for *S*-docosanylcysteine thin films on silicon substrates with native oxide layers. This analysis successfully provides information on the structural parameters and orientation of the molecular layer stack developed in *S*-docosanylcysteine thin films.

1. Introduction

Microscopy techniques such as transmission and scanning electron microscopy (TEM and SEM) and atomic force microscopy (AFM) have been widely used to explore nanostructures. However, when preparing sample specimens, TEM and SEM are destructive methods, and thus particular care should be taken to avoid possible damage to the specimens, especially for soft and/or polymeric materials. Moreover, the observed sample area is quite limited. AFM is a very powerful tool for observing surface topography of nanostructures (Yoon *et al.*, 2004), but it cannot be used to explore cross-sectional areas of sample specimens. Transmission neutron and X-ray scattering (TNS and TXS) methods have been widely used to determine the large-scale nanostructures of sample specimens (Shibayama & Hashimoto, 1986; Matsuoka *et al.*, 1987; Zheng *et al.*, 1989; Sakurai *et al.*, 1991; Hashimoto *et al.*, 1994; Mihailescu *et al.*, 2002; Lee, Shin *et al.*, 2004). In particular, these methods have been applied to characterize the structure and fluctuations of smectic membranes (de Jeu *et al.*, 2003). However, these techniques are not applicable for sample specimens on the nanometre scale, because of their poor sensitivity and resolution, which are attributed to the low scattering volumes. Thus, the development of a non-destructive method to analyze quantitatively the structures of suitably supported sample specimens on the nanometre scale is of great importance. Here, we introduce a grazing-incidence X-ray scattering (GIXS) technique that can be used to obtain highly intense scattering patterns with good counting statistics, even for very small sample specimens (Lee, Oh, Hwang *et al.*, 2005; Lee, Oh, Yoon *et al.*, 2005; Lee, Park, Hwang *et al.*, 2005; Lee, Park, Yoon *et al.*, 2005; Lee, Yoon *et al.*, 2005; Sinha *et al.*, 1988; Naudon, 1995; Tolan, 1999). Unlike conventional TXS and TNS, GIXS patterns need intensive analysis because of the complicated scattering nature caused by reflection and refraction effects (Lee, Park, Hwang *et al.*, 2005; Lee, Park, Yoon *et al.*, 2005; Lee, Yoon *et al.*, 2005).

In the present study, we derive a GIXS formula for an oriented molecularly stacked layer structure, and apply this formula to quantitatively analyze the GIXS patterns of *S*-docosanylcysteine thin films on silicon substrates. The GIXS measurements and data analysis were successfully carried out, providing detailed structural parameters and orientations of the *S*-docosanylcysteine thin film in a molecular layer stack.

2. Theory

The intensity of GIXS ($I_{\rm GIXS}$) from a thin film can be expressed using the following formula, which was recently derived with a distorted-wave Born approximation (Lee, Park, Yoon *et al.*, 2005; Lee, Yoon *et al.*, 2005):

$$I_{\rm GIXS}(\alpha_f, 2\theta_f) \cong \frac{1}{16\pi^2}\,\frac{1-\exp[-2{\rm Im}(q_z)d]}{2{\rm Im}(q_z)}\begin{bmatrix} \left|T_iT_f\right|^2 I_1(q_{||}, {\rm Re}(q_{1,z}))+ \\ \left|T_iR_f\right|^2 I_1(q_{||}, {\rm Re}(q_{2,z}))+ \\ \left|T_fR_i\right|^2 I_1(q_{||}, {\rm Re}(q_{3,z}))+ \\ \left|R_iR_f\right|^2 I_1(q_{||}, {\rm Re}(q_{4,z})) \end{bmatrix}, \tag{1}$$

where ${\rm Im}(q_z) = |{\rm Im}(k_{z,{\rm f}})| + |{\rm Im}(k_{z,{\rm i}})|$, ${\rm Re}(x)$ is the real part of x, d is the film thickness, $R_{\rm i}$ and $T_{\rm i}$ are the reflected and transmitted amplitudes of the incoming X-ray beam, respectively, and $R_{\rm f}$ and $T_{\rm f}$ are the reflected and transmitted amplitudes of the outgoing X-ray beam, respectively. In addition, $q_{||} = \sqrt{q_x^2 + q_y^2}$, $q_{1,z} = k_{z,{\rm f}} - k_{z,{\rm i}}$, $q_{2,z} = -k_{z,{\rm f}} - k_{z,{\rm i}}$, $q_{3,z} = k_{z,{\rm f}} + k_{z,{\rm i}}$ and $q_{4,z} = -k_{z,{\rm f}} + k_{z,{\rm i}}$; here, $k_{z,{\rm i}}$ is the z-component of the wavevector of the incoming X-ray beam, which is given by $k_{z,{\rm i}} = k_{\rm o}\sqrt{n_{\rm R}^2 - \cos^2\alpha_{\rm i}}$, and $k_{z,{\rm f}}$ is the z-component of the wavevector of the outgoing X-ray beam, which is given by $k_{z,{\rm f}} = k_{\rm o}\sqrt{n_{\rm R}^2 - \cos^2\alpha_{\rm f}}$, where $k_o = 2\pi/\lambda$, λ is the wavelength of the X-ray beam, $n_{\rm R}$ is the refractive index of the film given by $n_{\rm R} = 1 - \delta + i\xi$ with dispersion δ and absorption ξ, $\alpha_{\rm i}$ is the out-of-plane grazing-incidence angle of the incoming X-ray beam and $\alpha_{\rm f}$ is the out-of-plane exit angle of the out-going X-ray beam. q_x, q_y, and q_z are the components of the scattering vector $\mathbf{q}$. I_1 is the scattering intensity of the structure in the film, which can be calculated kinematically.

In equation (1), I_1 is the scattering intensity from the structure (*i.e.* scatterers and their ordering) in the film, which can be expressed by the following equation:

$$I_1(\mathbf{q}) = P(\mathbf{q}) \cdot S(\mathbf{q}), \tag{2}$$

where $P(\mathbf{q})$ is the form factor of the scatterers, which describes the shape, size, and orientation of the scatterers, and $S(\mathbf{q})$ is the structure

factor, which provides information on the positions of the scatterers, such as the crystal lattice parameters, orientation, dimension and symmetry in a crystalline solid and, in the case of an isotropic colloid-like system, the inter-distance of the scatterers.

To analyze quantitatively the molecular layer stack of the *S*-docosanylcysteine thin films in the present study, we have considered possible models including the Hosemann paracrystal model (Hosemann & Bagchi, 1962), the Cialle model (Liu & Nagle, 2004) and the modified Cialle model (Pabst *et al.*, 2000), and found that the paracrystal model is the most suitable for a layer lattice in our study, as shown in Fig. 1. For an ordered layer lattice with dimensions of L_1, L_2 and L_3, the form factor $P(\mathbf{q})$ can be expressed as follows (Zheng *et al.*, 1989):

$$P(\mathbf{q}) = \exp\left\{\frac{1}{4\pi}\left[L_1^2(q_x \sin\beta + q_z \cos\beta)^2 + L_2 q_y^2 + L_3 q_z^2\right]\right\} \sin^2\beta, \tag{3}$$

where q_x, q_y and q_z are the components of the scattering vector $\mathbf{q}$, and β is the angle between the $\mathbf{a}_1$ and $\mathbf{a}_3$ components of the lattice vector $\mathbf{a}$ (see Fig. 1). In this study, the lattice dimension is assumed to be identical to the inter-lattice distance, namely, $L_1 = L_2 = d_r$ and $L_3 = d_3$, where d_r is the lateral distance within a layer and d_3 is the long period between layers (see Fig. 1).

For a paracrystalline system, as proposed by Hosemann & Bagchi (1962) and refined by Blundell (1970), the structure factor $S(\mathbf{q})$ (the so-called interference function or lattice factor) can be determined from the Fourier transform of a complete set of lattice points. In the paracrystal model with distortion of the second kind, its lattice points are no longer fixed at certain positions, but are instead described by a positional distribution function. In the simple case, where the auto-correlation function of a crystal lattice is given by the convolution product of the lattice point distributions along the three vector component axes, and the distribution function is Gaussian, $S(\mathbf{q})$ can be expressed by the following equation (Wilke, 1983):

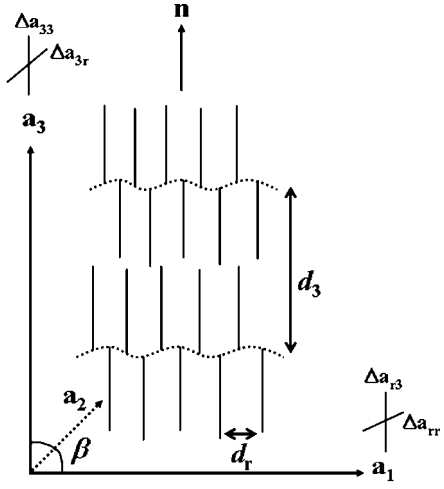

Figure 1
Schematic representation of a paracrystalline lattice composed of layer-ordered (*i.e.* lamellar-ordered) molecules. **a** is the primitive lattice vector, which is defined by its components, $\mathbf{a}_1$, $\mathbf{a}_2$ and $\mathbf{a}_3$, as shown in this figure; **n** is the vector of the layer orientation axis, which is parallel to $\mathbf{a}_3$; d_3 is the long period between layers; d_r is the lateral distance within a layer; β is the angle between $\mathbf{a}_1$ and $\mathbf{a}_3$; and Δa is the lattice positional fluctuation parameter. The subscript r denotes the direction transverse to $\mathbf{a}_3$. As an example, the molecule shown here in an extended chain in the layer-stacked structure assembly is *S*-docosanylcysteine, which was investigated in this study.

$$S(\mathbf{q}) = \prod_{k=1}^{3} Z_k(\mathbf{q}). \tag{4}$$

The kth lattice factor $Z_k(\mathbf{q})$ is given by:

$$Z_k(\mathbf{q}) = \frac{1 - |F_k(\mathbf{q})|^2}{1 + |F_k(\mathbf{q})|^2 - 2|F_k(\mathbf{q})|\cos(\mathbf{q}\cdot\mathbf{a}_k)}, \tag{5}$$

where

$$F_1(\mathbf{q}) = \exp\left[-\left(\frac{q_r^2 d_r^2 g_{rr}^2 + q_z^2 d_3^2 g_{r3}^2}{2}\right)\right] \tag{6a}$$

$$F_2(\mathbf{q}) = \exp\left[-\left(\frac{q_r^2 d_r^2 g_{rr}^2 + q_z^2 d_3^2 g_{r3}^2}{2}\right)\right] \tag{6b}$$

$$F_3(\mathbf{q}) = \exp\left[-\left(\frac{q_r^2 d_r^2 g_{3r}^2 + q_z^2 d_3^2 g_{33}^2}{2}\right)\right] \tag{6c}$$

and

$$\mathbf{q}\cdot\mathbf{a}_1 = (q_x + q_z \cot\beta) d_r \tag{7a}$$

$$\mathbf{q}\cdot\mathbf{a}_2 = q_y d_r \tag{7b}$$

$$\mathbf{q}\cdot\mathbf{a}_3 = q_z d_3, \tag{7c}$$

where $\mathbf{a}_k$ is the fundamental vector of the kth axis and $q_r = \sqrt{q_x^2 + q_y^2}$. g_{rr}, g_{rz}, g_{zr} and g_{zz} are the components of the paracrystal distortion factor, which are defined as:

$$g_{rr} = \Delta a_{rr}/a_r \tag{8a}$$

$$g_{r3} = \Delta a_{r3}/a_r \tag{8b}$$

$$g_{3r} = \Delta a_{3r}/a_r \tag{8c}$$

$$g_{33} = \Delta a_{33}/a_3, \tag{8d}$$

where Δa_k is the displacement of the vector $\mathbf{a}_k$ shown in Fig. 1; for example, Δa_{3r} represents the displacement of the fundamental vector $\mathbf{a}_3$ in the direction of r. In the present study, anisotropic displacement is assumed and the domain orientation is accounted for numerically.

For a layer structure with a given orientation, its fundamental vectors can be rotated and transformed using a rotation matrix. When the structure within a thin film is randomly oriented in-plane, but uniaxially oriented out-of-plane, the peak position vector $\mathbf{q}_c$ of a certain reciprocal lattice point $\mathbf{c}^*$ in the sample reciprocal lattice is given by:

$$\begin{aligned}\mathbf{q}_c &= \mathbf{R}\cdot\mathbf{c}^* \\ &\equiv (q_{c,x},\ q_{c,y},\ q_{c,z}),\end{aligned} \tag{9}$$

where $\mathbf{R}$ is a 3×3 matrix for deciding the preferred orientation of the structure in the film, and $q_{c,x}$, $q_{c,y}$ and $q_{c,z}$ are the x-, y- and z-components of the peak position vector $\mathbf{q}_c$, respectively. Using equation (9), every peak position can be determined. Due to the cylindrical symmetry, the Debye–Scherrer ring composed of the in-plane randomly oriented lattice point $\mathbf{c}^*$ transects the Ewald sphere at two points in the upper half of the sphere: $q_{||} = q_{c,||} \equiv \pm\sqrt{q_{c,x}^2 + q_{c,y}^2}$, with $q_z = q_{c,z}$. In this respect, diffraction patterns with cylindrical symmetry can easily be calculated in $\mathbf{q}$-space. It is then convenient to determine the preferred orientation of known structures and to analyze the anisotropic X-ray scattering patterns. However, since the $\mathbf{q}$-space in the GIXS patterns is distorted by refraction and reflection effects, the relation between the detector plane (expressed as the Cartesian coordinates defined by two

perpendicular axes, *i.e.* in-plane exit angle $2\theta_f$ and out-of-plane exit angle α_f) and the reciprocal lattice points is needed. The two wavevectors $k_{z,i}$ and $k_{z,f}$ are corrected for refraction as $k_{z,i} = k_o\sqrt{n_R^2 - \cos^2\alpha_i}$ and $k_{z,f} = k_o\sqrt{n_R^2 - \cos^2\alpha_f}$, respectively. Therefore, the two sets of diffractions that result from the incoming and outgoing X-ray beams, denoted by q_1 and q_3, respectively, are given at the exit angles by the following expression:

$$\alpha_f = \arccos\left(\sqrt{n_R^2 - \left(\frac{q_{c,z}}{k_o} \pm \sqrt{n_R^2 - \cos^2\alpha_i}\right)^2}\right), \qquad (10)$$

where $q_{c,z}/k_o > \sqrt{n_R^2 - \cos^2\alpha_i}$. In equation (10), the positive sign denotes diffractions produced by the outgoing X-ray beam, while the negative sign denotes diffractions produced by the incoming X-ray beam. The in-plane incidence angle $2\theta_i$ is usually zero, so the in-plane exit angle $2\theta_f$ can be expressed as:

$$2\theta_f = \arccos\left(\frac{\cos^2\alpha_i + \cos^2\alpha_f - \left(\frac{q_{c,\|}}{k_o}\right)^2}{2\cos\alpha_i\cos\alpha_f}\right). \qquad (11)$$

Therefore, diffraction spots observed at the detector plane in GIXS measurements can be compared directly with those derived using equations (9)–(11) from an appropriate model, and thus analyzed in terms of the model.

3. Experimental

3.1. Sample preparation

S-docosanylcysteine was synthesized from the reaction of cysteine and 1-bromodocosane as follows. Cysteine (2 g, 14.8 mmol) was dissolved in a mixture of 60 ml ethanol and 10 ml aqueous NaOH (2.0 *N*) and stirred at room temperature for 30 min. 1-Bromodocosane (7.5 g, 19.2 mmol) was then added and the solution was stirred for an additional 6 h at room temperature. The reaction mixture was poured into cold water and its pH value was adjusted to 7.0, precipitating *S*-docosanylcysteine as a white powder in 76% yield. The product was then filtered off, washed several times with distilled deionized water and dried in a vacuum oven at room temperature. The dried *S*-docosanylcysteine product was dissolved in chloroform containing a few drops of trifluoroacetic acid, producing a solution of 2 wt%. This solution was filtered through PTFE membranes of pore size 0.2 µm and then spin-coated onto pre-cleaned silicon substrates at 2000 rpm for 30 s, followed by drying at 323 K for 1 d under vacuum. The thickness of the obtained films (80–90 nm) was measured using spectroscopic ellipsometry. All materials and solvents were purchased from Aldrich Chemical Company and used as received.

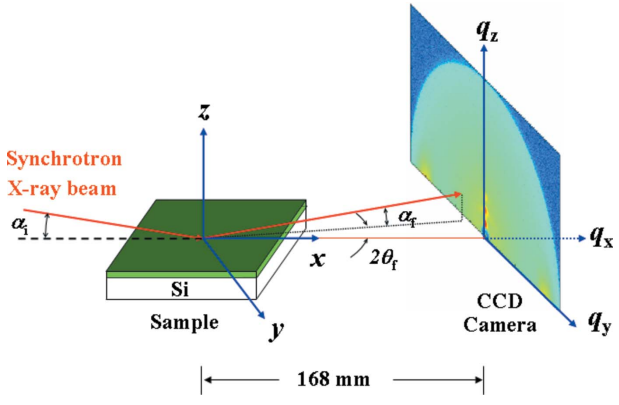

Figure 2
Geometry of GIXS. α_i is the incident angle at which the X-ray beam impinges on the film surface; α_f and $2\theta_f$ are the exit angles of the X-ray beam with respect to the film surface and to the plane of incidence, respectively, and q_x, q_y and q_z are the components of the scattering vector **q**.

3.2. GIXS measurement

GIXS measurements were carried out at the 4C1 and 4C2 beamlines (Bolze *et al.*, 2002, 2001; Yu *et al.*, 2005) at the Pohang Accelerator Laboratory (Ree & Ko, 2005). The samples were measured at a sample-to-detector distance of 168 mm using an X-ray radiation source of λ = 0.154 nm and imaged using a two-dimensional charge-coupled detector (two-dimensional CCD; Roper Scientific, Trenton, NJ, USA), as shown in Fig. 2. Samples were mounted on a home-made *z*-axis goniometer equipped with a vacuum chamber. The incidence angle α_i of the X-ray beam was set at 0.20°, which is between the critical angles of the films and the silicon substrate ($\alpha_{c,f}$ and $\alpha_{c,s}$). Scattering angles were corrected according to the positions of the X-ray beams reflected from the silicon substrate interface with changing incidence angle α_i and with respect to a pre-calibrated silver behenate powder (TCI, Japan). Aluminium foil pieces were employed as semi-transparent beam stops, because the intensity of the specular reflection from the substrate is much stronger than the intensity of GIXS near the critical angle. Data were typically collected for 10 s.

4. Results and discussion

Using the equations derived in Section 2, the following numerical GIXS simulations were conducted for a thin film composed of a layer of paracrystals randomly oriented in the plane of the film, but uniaxially oriented out of the film plane, in order to understand the relationships of the structural parameters with respect to the resulting GIXS pattern. Representative results are shown in Fig. 3.

Figs. 3(*a*) and (*b*) show $I_{GIXS}(\mathbf{q})$ profiles for a layer structure defined by paracrystalline parameters of d_r = 0.425 nm, d_3 = 3.00 nm, β = 90° and various *g* factors. In this calculation, anisotropic distortion is assumed, and therefore the value of the *g* factor is unique according to the displacement direction. For a small g_{33} value (0.03), many sharp peaks appear in the $I_{GIXS}(\mathbf{q})$ profile, which are all characteristic diffractions of the layer-stacked structure (Fig. 3*a*). Here, these peaks are assigned by the (001), (002), (003), (004), (005) and (006) diffractions in the order of low to high q_{xy}, whose relative scattering vector lengths from the specular reflection position are integer orders of the first peak. As the *g* factor increases, these diffraction peaks become noticeably weaker and broader (Fig. 3*a*). In the case of the in-plane GIXS profile along the $2\theta_f$ direction, the resulting diffraction peaks also become weaker and broader with increasing g_{rr} factor (Fig. 3*b*). Thus, this kind of distortion causes the intensity amplitudes of the Bragg diffraction peaks to decrease and the broadness of the diffraction peaks to increase; such peak broadness becomes much more severe for the higher order diffraction peaks. In conclusion, the vectors of adjacent lattice cells vary in magnitude and direction due to the displacement of the lattice points from their proper positions, ultimately resulting in a loss of long-range order in the paracrystal. Therefore, these *g*-factor simulations can provide an experimental basis for determining the degree of lattice distortion of a chosen paracrystalline system, and furthermore its lattice dimension parameters can be determined from the diffraction peak positions.

Figs. 3(*c*) and (*d*) show the influences of the lattice dimensions d_3 and d_r on the $I_{GIXS}(\mathbf{q})$ profile with $g_{33} = 0.05$ and $g_{rr} = 0.1$. As can be seen in these figures, both the d_3 and d_r values directly affect the positions of the peaks; the peak positions are sensitively changed by varying the lattice size in accordance with Bragg's relation. Since the incident angle α_i of the X-ray beam is relatively small, the GIXS signal mainly depends on both the in-plane scattering vector component q_{xy}, which is related to the lateral ordering d_r in the layer structure, and the out-of-plane scattering vector component q_z which is related to d_3, namely the ordering in the thickness direction of the film. Thus, this analysis can provide a basis for the experimental determination of the lattice dimensions d_3 and d_r.

To determine the relation between the orientation of a paracrystal lattice (which is described by the rotation matrix **R** discussed in Section 2) and the GIXS pattern, we attempted to calculate two-dimensional GIXS patterns using the GIXS formula. Fig. 4 shows two-dimensional patterns of the $I_{GIXS}(\mathbf{q})$ profiles, which were calculated with varying rotation matrix **R** values. In these calculations, several parameters were fixed; $d_3 = 2.0$ nm, $g_{33} = 0.09$, $g_{3r} = 0.05$, $d_r = 0.8$ nm, $g_{r3} = 0.15$, $g_{rr} = 0.15$, $\beta = 90$ and $\alpha_i = 0.20°$. Fig. 4(*a*) shows the GIXS pattern for a layer-stacked structure, which assumes that the **n** vector is perfectly oriented normal to the film plane (see the model in the inset). As can be seen in Fig. 4(*a*), specular reflections appear at α_f = 4.4, 8.8, and 13.2° (in integer orders of the first peak) along the α_f direction in accordance with the d_3 value of 2.0 nm. Since the value of d_r is smaller than that of d_3, and the g_{rr} value of 0.15 is larger than g_{33}, only one broad peak (whose peak maximum is at $2\theta_f = 11.1°$) appears at $\alpha_f = 0°$ along the $2\theta_f$ direction. When the **n** vector lies parallel to the film plane, specular reflections due to d_3 appear at $\alpha_f = 0°$ along the $2\theta_f$ direction, where one broad peak (whose peak maximum is at α_f = 11.1°) appears at $2\theta_f = 0°$ along the α_f direction (Fig. 4*b*). Thus, these orthogonal relations between the GIXS patterns in Figs. 4(*a*) and (*b*) result from the preferred orientations of the layer-stacked structure in the film. When the **n** vector is randomly oriented within the film, the calculated GIXS pattern shows isotropic scattering rings (so-called Debye–Scherrer rings) at 4.4, 8.8, 11.1, and 13.2°, rather than scattering peaks, as shown in Fig. 4(*c*). The scattering ring at 11.1° comes from the first-order peak of the d_r lattice, while the other rings come from the first-order and higher-order peaks of the d_3 lattice.

The distribution of the orientation vector **n** with respect to the film plane is given by a function $D(\varphi)$, where φ is the polar angle between the **n** vector and the out-of-plane direction of the film; for example, φ is zero when the **n** vector in the film is perfectly oriented normal to the film plane. To calculate the two-dimensional GIXS patterns, $D(\varphi)$ should be represented by an actual numerical function. In relation to the distribution of the lattice orientation, $D(\varphi)$ can generally be considered as a Gaussian distribution:

$$D(\varphi) = \frac{1}{\sqrt{2\pi}\sigma_\varphi} \exp\left[-\frac{(\varphi - \overline{\varphi})^2}{2\sigma_\varphi^2}\right] \qquad (12)$$

where $\overline{\varphi}$ and σ_φ are the mean angle and standard deviation of φ from $\overline{\varphi}$, respectively. The observed scattering intensity $I_{GIXS,\varphi}(\mathbf{q})$ is obtained by averaging $I_{GIXS}(\mathbf{q})$ over possible orientations of the lattice:

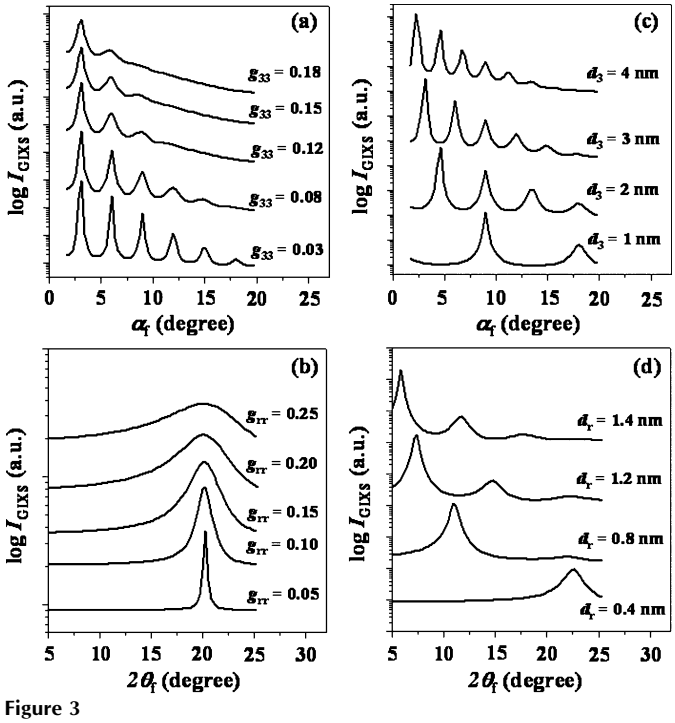

Figure 3
$I_{GIXS}(\mathbf{q})$ profiles for a layer-stacked structure (which is defined by paracrystalline parameters of $d_r = 0.425$ nm, $d_3 = 3.00$ nm and $\beta = 90°$) with various *g* factors; (*a*) g_{33} = 0.03, 0.08, 0.12, 0.15 and 0.18; (*b*) g_{rr} = 0.05, 0.10, 0.15, 0.20 and 0.25. Influences of the lattice dimensions d_3 and d_r on $I_{GIXS}(\mathbf{q})$ profiles with $g_{33} = 0.05$ and $g_{rr} = 0.1$; in this calculation, the d_3 and d_r values vary in the range 1−4 nm (*c*) and 0.4−1.4 nm (*d*), respectively.

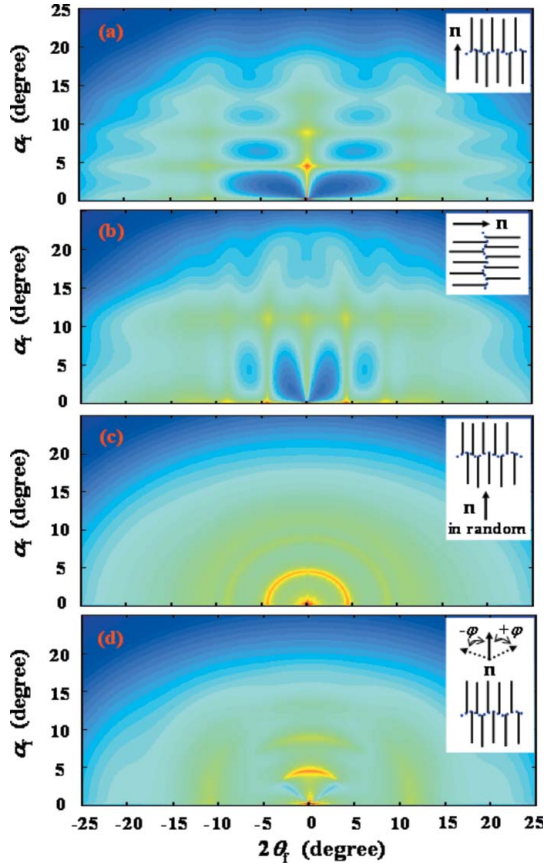

Figure 4
Two-dimensional patterns of the $I_{GIXS}(\mathbf{q})$ profile, which were calculated with varying rotation matrix **R** values. In these calculations, we fixed several parameters: $d_3 = 2.0$ nm, $g_{33} = 0.09$, $g_{3r} = 0.05$, $d_r = 0.8$ nm, $g_{r3} = 0.15$, $g_{rr} = 0.15$, $\beta = 90°$ and α_i = 0.20°. (*a*) Pattern for thin films which assumed that the **n** vector in the film is perfectly oriented normal to the film plane (see the model in the inset); (*b*) the **n** vector lies perfectly parallel to the film plane (model shown in inset); (*c*) the **n** vector is randomly oriented within the film (model shown in inset); (*d*) the **n** vector has a distribution which follows a Gaussian function ($\overline{\varphi} = 0°$ and $\sigma_\varphi = 15°$ in equation 12) (model shown in inset).

$$I_{\mathrm{GIXS},\varphi}(\mathbf{q}) = \int_{-\pi}^{\pi} I_{\mathrm{GIXS}}(\mathbf{q}) D(\varphi) \mathrm{d}\varphi \qquad (13)$$

Fig. 4(*d*) shows a two-dimensional GIXS pattern, which was calculated by averaging $I_{\mathrm{GIXS}}(\mathbf{q})$ with an orientation distribution function $D(\varphi)$. For this calculation, the same structural parameters used for the GIXS pattern in Fig. 4(*a*) were also applied here, with $\overline{\varphi} = 0^\circ$ and $\sigma_\varphi = 15^\circ$ (see the φ distribution in the inset). As can be seen in Fig. 4(*d*), the calculated GIXS pattern reveals arcs rather than sharp spots, which are formed by linking the diffraction spots from the same family of lattice planes with distributed orientations. With increasing σ_φ value, the scattering arcs become more circular, and ultimately form rings with a completely random orientation. As can be seen in Fig. 4(*d*), specular reflections appear at $\alpha_\mathrm{f} = 4.4$, 8.8, and 13.2° as arcs distributed along the $2\theta_\mathrm{f}$ direction, whereas specular reflections resulting from d_r appear distributed along the α_f direction. Collectively, this analysis method can provide information about the preferred orientation and the distribution of the determined layer-stacked structure and, moreover, it can also be used to characterize anisotropic GIXS patterns quantitatively.

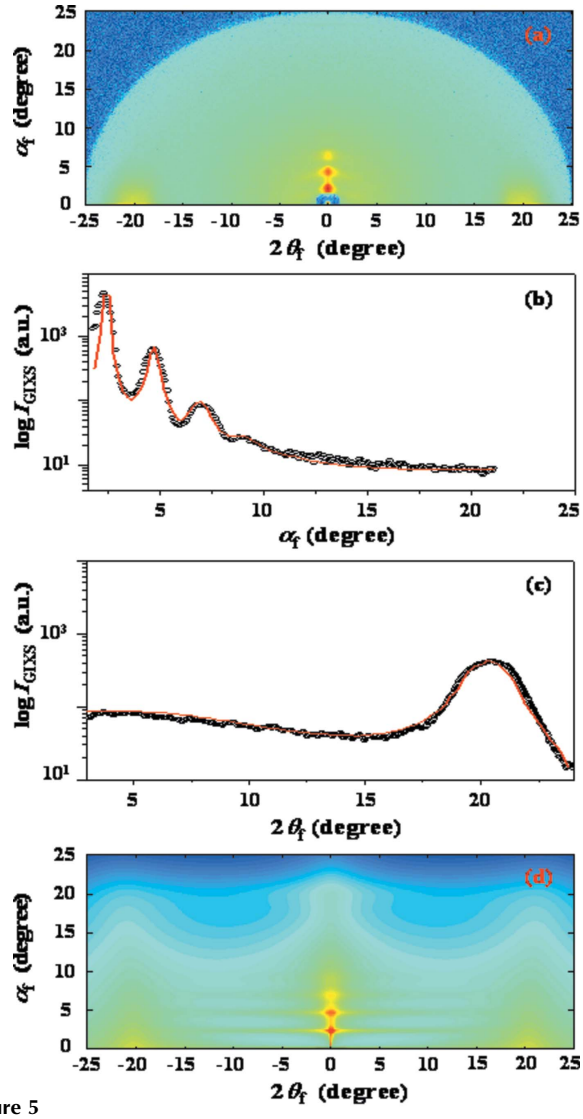

Figure 5
(*a*) Two-dimensional GIXS pattern measured at $\alpha_\mathrm{i} = 0.20^\circ$ for an *S*-docosanylcysteine thin film deposited on a silicon substrate. (*b*) Out-of-plane scattering profile extracted from the GIXS pattern in (*a*) along the α_f direction at $2\theta_\mathrm{f} = 0^\circ$. (*c*) In-plane scattering profile extracted from the GIXS in (*a*) along the $2\theta_\mathrm{f}$ direction at $\alpha_\mathrm{f} = 0.20^\circ$. The open circles in (*b*) and (*c*) represent the measured data, while the solid lines were obtained by fitting the data according to the GIXS formula. (*d*) A calculated two-dimensional GIXS pattern with structural parameters (listed in Table 1) obtained by analyzing the GIXS data in (*a*), using the derived formula.

Table 1
Structural parameters of the *S*-docosanylcysteine thin film, which were obtained by GIXS measurements and data analysis.

d_3	d_r	g_{33}	$g_{3\mathrm{r}}$	$g_{\mathrm{r}3}$	g_{rr}	β	$\overline{\varphi}$	σ_φ
3.80 nm	0.44 nm	0.085	0.025	0.25	0.11	90.0°	0.0°	2.0°

Here, we apply the GIXS analysis method to analyze quantitatively two-dimensional GIXS patterns measured for *S*-docosanylcysteine thin films supported on silicon substrates. As can be seen in the representative two-dimensional GIXS pattern shown in Fig. 5(*a*), strong specular reflections appear along the α_f direction and, in contrast, one broad peak appears along the $2\theta_\mathrm{f}$ direction at $\alpha_\mathrm{f} = 0^\circ$, whose peak maximum is around $2\theta_\mathrm{f} = 20^\circ$. These scattering peaks suggest that the layers are well developed and stacked together along the direction normal to the film plane (*i.e.* the orientation vector **n** lies normal to the film plane), although the lateral packing order in the layers is very poor.

Taking this qualitative structural information into account, the out-of-plane and in-plane scattering profiles in the GIXS patterns in Fig. 5(*a*) have been extracted from along the α_f direction at $2\theta_\mathrm{f} = 0^\circ$ and along the $2\theta_\mathrm{f}$ direction at $\alpha_\mathrm{f} = 0.20^\circ$, respectively, and plotted in Figs. 5(*b*) and (*c*). As can be seen in Fig. 5(*b*), the out-of-plane profile clearly reveals four diffraction spots, whose relative scattering vector lengths from the specular reflection position are 1, 2, 3, and 4; in fact, the fourth spot is very weak in intensity compared with the other spots. In contrast, the in-plane scattering profile is quite different from the out-of-plane profile. Specifically, the in-plane profile reveals only one broad peak at $2\theta_\mathrm{f} = 20.5^\circ$ (Fig. 5*c*). These scattering profiles can be fitted satisfactorily with the GIXS formula derived in Section 2 (Figs. 5*b* and *c*). These analyses provided all the structural details of the *S*-docosanylcysteine thin film. The extracted structural parameters, including the lattice positional distortions, the orientation and its distribution, are summarized in Table 1.

From these GIXS data analyses, the *S*-docosanylcysteine thin film was found to be composed of molecularly well assembled multilayers, whose layers are stacked out of the plane of the film. The mean layer thickness is 3.80 nm (= d_3) and the mean lateral inter-distance of the fully extended molecules in the paracrystals within the layer is 0.44 nm (= d_r). The observed mean layer thickness is longer than the length of a fully extended *S*-docosanylcysteine molecule (2.98 nm), but much shorter than twice the length of a fully extended molecule. In fact, the length of the fully extended *S*-docosanylcysteine molecule consists of a polar cysteine head (0.50 nm in length) and a non-polar *n*-docosanyl tail (2.48 nm in length). Taking into account these head and tail sizes, the observed mean layer thickness indicates that the fully extended *S*-docosanylcysteine molecules are interdigitated along the longitudinal direction of the molecule *via* the favourable interaction of the *n*-docosanyl tails, which are longer than the length of the polar cysteine heads, resulting in the formation of a layer of paracrystals in the film. Here, it is noteworthy that the *n*-docosanyl tails are fully interdigitated with the paracrystals in the layer structure.

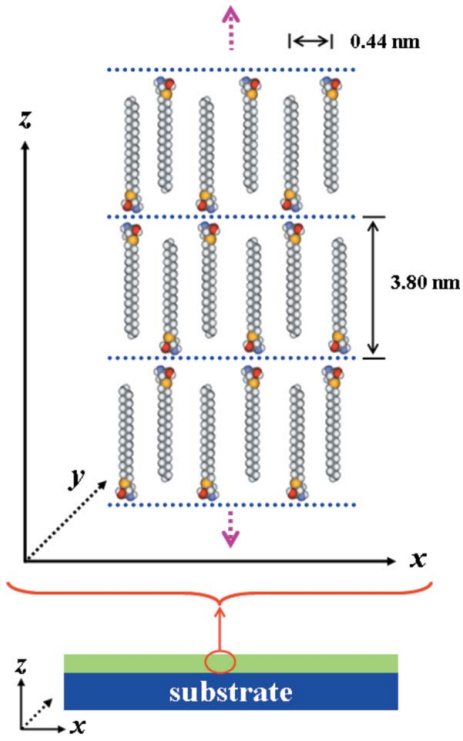

Figure 6
Schematic representation of a layer-stacked structure (*i.e.* lamellar structure) formed in the *S*-docosanylcysteine thin film on a silicon substrate. Each layer consists of paracrystals of fully extended *S*-docosanylcysteine molecules with interdigitated *n*-docosanyl tails.

The positional disorder of the *S*-docosanylcysteine paracrystals out of the plane of the film is very small: $g_{33} = 0.085$ and $g_{3r} = 0.025$. Moreover, the mean orientation angle $\overline{\varphi}$ with respect to the out-of-plane projection is 0.0° and its deviation σ_{φ} is only 2.0°; it is also found that $\beta = 90.0°$. These results collectively indicate that the self-assembled layers consisting of *S*-docosanylcysteine paracrystals are stacked perfectly normal to the film plane. The results further indicate that there is almost no undulation at each layer surface. In comparison with the positional disorder along the out-of-plane projection, the positional disorder of the *S*-docosanylcysteine paracrystals in the film plane is, however, relatively large: $g_{r3} = 0.25$ and $g_{rr} = 0.11$. These relatively large g_{r3} and g_{rr} values indicate that the *S*-docosanylcysteine molecules are poorly packed together in the paracrystals formed within each layer structure. This poor lateral packing characteristic may further lead to a tendency to form microdomains composed of *S*-docosanylcysteine paracrystals in the film plane; this possibility, however, requires more detailed study.

With the structural parameters determined here, we have fitted two-dimensional GIXS patterns using the GIXS formula, as displayed in Fig. 5(*d*). The calculated GIXS pattern is found to match well with the experimentally measured scattering pattern in Fig. 5(*a*).

From the measured GIXS data and the quantitative data analysis results, we propose a structural model for the *S*-docosanylcysteine thin film deposited on silicon substrates, as shown in Fig. 6.

5. Conclusions

We have derived a GIXS formula for layer-stacked structures in nano-sized thin films supported on silicon substrates. A comprehensive numerical analysis using the derived formula has been performed for a layer-stacked structure in thin films formed on substrates. Furthermore, the derived scattering formula has been used to analyze the two-dimensional GIXS patterns measured for *S*-docosanylcysteine thin films supported on silicon substrates.

The quantitative analysis of the measured GIXS patterns using the derived formula has been successfully demonstrated. Indeed, this analysis establishes that, in the thin film, the *S*-docosanylcysteine molecules self-assemble as a fully extended chain *via* strong interdigitation of the *n*-docosanyl tails and the favourable interaction of the polar cysteine heads, which combine to form layers of paracrystals that are stacked perfectly normal to the film plane. Moreover, this analysis has provided structural parameter details of the thin film.

This study was supported by the Korea Science and Engineering Foundation (National Research Laboratory Program and Center for Integrated Molecular Systems) and by the Ministry of Education (BK21 Program). Synchrotron GIXS measurements at the Pohang Accelerator Laboratory were supported by the Ministry of Science and Technology and the POSCO.

References

Blundell, D. J. (1970). *Acta Cryst.* A**26**, 472–476; 476–483.
Bolze, J., Kim, J., Huang, J.-Y., Rah, S., Youn, H. S., Lee, B., Shin, T. J. & Ree, M. (2002). *Macromol. Res.* **10**, 2–12.
Bolze, J., Ree, M., Yoon, H. S., Chu, S.-H. & Char, K. (2001). *Langmuir*, **17**, 6683–6691.
Hashimoto, T., Kawamura, T., Harada, M. & Tanaka, H. (1994). *Macromolecules*, **27**, 3063–3072.
Hosemann, R. & Bagchi, S. N. (1962). *Direct Analysis of Diffraction by Matter*. Amsterdam: North-Holland.
Jeu, W. H. de, Ostrovskii, B. I. & Halaginov, A. N. (2003). *Rev. Mod. Phys.*, **75**, 181–235.
Lee, B., Oh, W., Hwang, Y., Park, Y.-H., Yoon, J., Jin, K. S., Heo, K., Kim, J., Kim, K.-W. & Ree, M. (2005). *Adv. Mater.* **17**, 696–701.
Lee, B., Oh, W., Yoon, J., Hwang, Y., Kim, J., Landes, B. G., Quintana, J. P. & Ree, M. (2005). *Macromolecules*, **38**, 8991–8995.
Lee, B., Park, I., Yoon, J., Park, S., Kim, J., Kim, K.-W., Chang, T. & Ree, M. (2005). *Macromolecules*, **38**, 4311–4323.
Lee, B., Park, Y.-H., Hwang, Y.-T., Oh, W., Yoon, J. & Ree, M. (2005). *Nat. Mater.* **4**, 147–150.
Lee, B., Shin, T. J., Lee, S. W., Yoon, J., Kim, J. & Ree, M. (2004). *Macromolecules*, **37**, 4174–4184.
Lee, B., Yoon, J., Oh, W., Hwang, Y.-T., Heo, K., Jin, K. S., Kim, J., Kim, K.-W. & Ree, M. (2005). *Macromolecules*, **38**, 3395–3405.
Liu, Y. & Nagle, J. F. (2004). *Phys. Rev. E*, **69**, 040901 (1–4).
Matsuoka, H., Tanaka, H., Hashimoto, T. & Ise, N. (1987). *Phys. Rev. B*, **36**, 1754–1765.
Mihailescu, M., Monkenbusch, M., Allgaier, J., Feielinghaus, H., Richter, D., Jakobs, B. & Sottmann, T. (2002). *Phys. Rev. E*, **66**, 041504 (1–13).
Naudon, A. (1995). *Modern Aspects of Small-Angle Scattering*. Amsterdam: Kluwer Academic Publishers.
Pabst, G., Rappaolt, M., Amenitsch, H. & Laggner, P. (2000). *Phys. Rev. E*, **62**, 4000–4009.
Ree, M. & Ko, I. S. (2005). *Phys. High Tech.* **14**, 2–7.
Sakurai S., Okamoto, S., Kawamura, T. & Hashimoto, T. (1991). *J. Appl. Cryst.* **24**, 679–684.
Shibayama, M. & Hashimoto, T. (1986). *Macromolecules*, **19**, 740–749.
Sinha, S. K., Sirota, E. B., Garoff, S. & Stanley, H. B. (1988). *Phys. Rev. B*, **38**, 2297–2311.
Tolan, M. (1999). *X-ray Scattering from Soft Matter Thin Films*. Berlin: Springer.
Wilke, W. (1983). *Acta Cryst.* A**39**, 864–867.
Yoon, J., Ree, M., Hwang, Y., Lee, S., Lee, B., Kim, J.-S., Kim, H. & Magonov, S. N. (2004). *Langmuir*, **20**, 544–549.
Yu, C.-J., Kim, J., Kim, K.-W., Kim, G.-H., Lee, H.-S., Ree, M. & Kim, K.-J. (2005). *J. Kor. Vac. Soc.* **14**, 138–142.
Zheng, Z., Nojima, S., Yamane, T. & Ahida, T. (1989). *Macromolecules*, **22**, 4362–4367.